

## Photoabsorption spectra of I and its ions in the 4*d* region

A. T. Domondon<sup>1,\*</sup> and X. M. Tong<sup>2</sup>

<sup>1</sup>*Division of Natural Sciences, International Christian University, Ohsawa, Mitaka-shi, Tokyo 181-8585, Japan*

<sup>2</sup>*“Cold Trapped Ions” Project, ICORP, JST, Axis 3F, 1-40-2 Fuda Chofu, Tokyo 182-0024, Japan*

(Received 2 February 2001; published 22 February 2002)

We have studied the 4*d* photoabsorption process of I, I<sup>+</sup>, I<sup>2+</sup>, and I<sup>3+</sup> by using linear density-response theory together with density-functional theory to take into account the dynamic electron correlation, which is crucially important in reproducing the 4*d* giant resonance. The current approach, however, differs from previous approaches of this type in that we use an optimized effective potential and explicitly incorporate a self-interaction correction. We found that the 4*d* photoabsorption spectrum of the I<sup>+</sup> ion is almost the same as that of the neutral I atom, and that in moving from I to I<sup>3+</sup> the spectrum changes from one notably characterized by a giant resonance into one with multiple sharp peaks. Convoluting the spectra with the experimental energy resolution yielded spectra in excellent agreement with absolute experimental photoabsorption cross-section spectra. Moreover, our results showed better agreement with experiment than earlier theoretical studies. In addition, increasing the energy resolution revealed peaks not observed in the experimental spectra.

DOI: 10.1103/PhysRevA.65.032718

PACS number(s): 32.80.Fb, 31.15.Ew

### I. INTRODUCTION

The 4*d* giant resonance seen in the photoabsorption spectra of rare-gas atoms and their ions have long been a subject of interest in atomic physics [1–3]. In particular, the I atom and its ions have lately attracted much attention. This interest stems from the fact that in the Periodic Table, I is positioned next to Xe, an atom for which giant resonance processes have been well studied. Although some theoretical and experimental work has been done on I and its ions, there has been considerable disagreement between theory and experiment. Recent work on I has included a theoretical attempt by Amusia *et al.* [6] to calculate the 4*d* photoabsorption cross section of the I atom and its ions using the random-phase approximation with exchange (RPAE). They noted that their cross-section values were three times larger than previous experimental values obtained through normalization of relative cross-section measurements by O’Sullivan *et al.* [5] and Nahon *et al.* [4]. The most recent experiment due to Kjeldsen *et al.* [7], however, measured the absolute photoabsorption cross section of the same species and obtained results that suggest that theoretical calculations are 30–40% too large. This work attempts to clarify this discrepancy by calculating the cross section of I and its ions by invoking linear-response theory and density-functional theory, but improves upon conventional implementations of those theories by using an optimized effective potential and incorporating a self-interaction correction. Henceforth, we shall refer to this approach as the time-dependent local-density spin approximation with an optimized effective potential and self-interaction correction (TDLSDA/OEP-SIC). The justification for this approach comes from the theoretical understanding that the giant 4*d* photoabsorption cross section for rare-gas atoms is due to the electron-electron dynamic correlation and the double-well potential for the final *f* partial wave [3,8,9]. Hence, any approach that hopes to reproduce successfully

the 4*d* giant resonance must thoroughly take into account the electron-electron dynamic correlation. Moreover, the extent to which the giant resonance appears in the spectrum depends on the electron-nucleus Coulombic interaction and electron-electron correlation. In fact, it is known that increasing the degree of ionization obscures the giant resonance effect by inducing an “orbital collapse” of the *f* partial wave [3,8], and hence for highly charged ions their spectrum is characterized by sharp resonance lines rather than a giant resonance [10,11]. This tendency was also confirmed in the current calculated spectra for I, I<sup>+</sup>, I<sup>2+</sup>, and I<sup>3+</sup>. In addition, convoluting our calculated results for I<sup>+</sup> and I<sup>2+</sup> using the experimental energy resolution employed in the most recent experimental work [7] yielded excellent agreement between the two. The theoretical spectra also revealed some spectral lines unresolved in the experiment. Theoretically, our results represent an improvement over the previous theoretical calculations done employing RPAE [6]. In particular, RPAE overestimates the cross-section values by about 30–40%, whereas our calculations give cross-section values well within the error range of the experiment. We will give a brief description of our theoretical method in Sec. II, and present our results and a discussion in Sec. III.

### II. THEORETICAL METHOD

The theoretical method used in the present calculation follows that employed in Ref. [12]. In particular, we stress that the method improves upon other density-functional approaches in that it uses an optimized effective potential and incorporates a self-interaction correction. Given an initial state  $|is\rangle$  and a final state  $|js\rangle$  where *s* is the spin index (spin up ↑ or spin down ↓), the photoabsorption cross section from one state to the other can be expressed as (atomic units  $\hbar = m = e = 1$  are used throughout unless explicitly stated otherwise)

$$\sigma_{is}(\omega) = \frac{2\omega}{3} \frac{2\pi^2}{c} n_{is} \sum_{js} (1 - n_{js}) |\langle js | \mathbf{r} | is \rangle|^2 \times \delta(\omega - \epsilon_{js} + \epsilon_{is}), \quad (1)$$

\*Email address: domondon@icu.ac.jp

where  $|is\rangle$  and  $|js\rangle$  are the solutions of the one-electron Schrödinger-like equation

$$\left[ -\frac{1}{2}\nabla^2 + V_s^{\text{eff}}(\mathbf{r}) \right] \phi_{is}(\mathbf{r}) = \epsilon_{is} \phi_{is}(\mathbf{r}). \quad (2)$$

Here  $V_s^{\text{eff}}(\mathbf{r})$  is a spin-dependent effective potential. The final states are unbound solutions of Eq. (2) with  $\epsilon_{is}$  replaced by  $\frac{1}{2}k^2$ , where  $k$  is the photoelectron momentum and  $n_{is}$  and  $n_{js}$  are the occupation number of the initial and final states, respectively. This type of independent-particle approximation (IPA) does not take into account the electron dynamic correlation. Consequently, the calculated photoabsorption cross section near the giant resonance cannot fully reproduce the experimental observations [13]. Moreover, the IPA model does not take into account the interaction between the photoexcitation and the photoabsorption from different shells. One way to take into account the dynamic electron correlation ignored in the IPA model is to invoke linear density-response theory [13–17]. In particular, linear response density theory allows one to incorporate the effect of a weak time-dependent perturbation field on the electron density.

The frequency-dependent induced density  $\delta\rho(\mathbf{r},\omega)$  can be obtained by the Fourier transformation of the time-dependent field-induced density  $\delta\rho(\mathbf{r},t)$ :

$$\delta\rho(\mathbf{r},\omega) = \frac{1}{2\pi} \int_{-\infty}^{\infty} \delta\rho(\mathbf{r},t) e^{i\omega t} dt. \quad (3)$$

The induced density is related to an external field by

$$\delta\rho(\mathbf{r},\omega) = \int \chi(\mathbf{r},\mathbf{r}',\omega) V^{\text{ext}}(\mathbf{r}',\omega) d^3\mathbf{r}', \quad (4)$$

where  $\chi(\mathbf{r},\mathbf{r}',\omega)$  is the frequency-dependent susceptibility and

$$V^{\text{ext}}(\mathbf{r},\omega) = z \quad (5)$$

is the dipole external field. The susceptibility can be determined by means of the first-order time-dependent perturbation theory [18] and expressed in terms of the eigenfunctions  $\{\phi_{is}(\mathbf{r})\}$  and eigenvalues  $\{\epsilon_{is}\}$  of the solutions of Eq. (2) as

$$\chi_s^{\text{IPA}}(\mathbf{r},\mathbf{r}',\omega) = \sum_{is,j_s} (n_{is} - n_{j_s}) \frac{\phi_{is}^*(\mathbf{r}) \phi_{j_s}(\mathbf{r}) \phi_{is}(\mathbf{r}') \phi_{j_s}^*(\mathbf{r}')}{\omega - (\epsilon_{j_s} - \epsilon_{is}) + i\eta}. \quad (6)$$

Here  $i\eta$  is an imaginary infinitesimal used to ensure the outgoing wave boundary condition. Note that the  $\eta$  can also be treated as the experimental energy resolution with the Lorentzian line profile. The summation over  $i$  and  $j$  runs over all the bound and continuum states. Since the change of the electron density will result in a local field correction, the effective field or self-consistent field (SCF)  $V_s^{\text{SCF}}(\mathbf{r},\omega)$  can be obtained by replacing Eq. (4) with

$$\begin{aligned} \delta\rho(\mathbf{r},\omega) &= \sum_s \int \chi_s^{\text{IPA}}(\mathbf{r},\mathbf{r}',\omega) V_s^{\text{SCF}}(\mathbf{r}',\omega) d^3\mathbf{r}' \\ &= \sum_s \delta\rho_s(\mathbf{r},\omega). \end{aligned} \quad (7)$$

We use the IPA potential obtained from the density-functional theory with an optimized effective potential and a self-interaction correction [19,20]. With such an IPA potential,  $V_s^{\text{SCF}}(\mathbf{r},\omega)$  can be expressed as

$$\begin{aligned} V_s^{\text{SCF}}(\mathbf{r},\omega) &= V^{\text{ext}}(\mathbf{r},\omega) + \int \frac{\delta\rho(\mathbf{r}',\omega)}{|\mathbf{r}-\mathbf{r}'|} \\ &\quad \times d^3\mathbf{r}' + \frac{\partial V_{\text{xc}}(\mathbf{r})}{\partial\rho_s(\mathbf{r})} \Big|_{\rho_o(\mathbf{r})} \delta\rho_s(\mathbf{r},\omega). \end{aligned} \quad (8)$$

Here  $\rho_o(\mathbf{r})$  is the ground-state electron density. The normal procedure is to solve Eqs. (7) and (8) iteratively until convergence is reached. An alternative and simpler procedure, however, can be obtained by substituting Eq. (7) into Eq. (8) to get

$$\begin{aligned} \begin{bmatrix} V_{\uparrow}^{\text{SCF}}(\mathbf{r},\omega) \\ V_{\downarrow}^{\text{SCF}}(\mathbf{r},\omega) \end{bmatrix} &= \begin{bmatrix} V^{\text{ext}}(\mathbf{r},\omega) \\ V^{\text{ext}}(\mathbf{r},\omega) \end{bmatrix} + \int \begin{bmatrix} K_{\uparrow\uparrow}(\mathbf{r},\mathbf{r}') & K_{\uparrow\downarrow}(\mathbf{r},\mathbf{r}') \\ K_{\downarrow\uparrow}(\mathbf{r},\mathbf{r}') & K_{\downarrow\downarrow}(\mathbf{r},\mathbf{r}') \end{bmatrix} \\ &\quad \times \begin{bmatrix} V_{\uparrow}^{\text{SCF}}(\mathbf{r}',\omega) \\ V_{\downarrow}^{\text{SCF}}(\mathbf{r}',\omega) \end{bmatrix} d^3\mathbf{r}', \end{aligned} \quad (9)$$

with

$$\begin{aligned} K_{\uparrow\uparrow}(\mathbf{r},\mathbf{r}') &= \int \frac{\chi_{\uparrow}^{\text{IPA}}(\mathbf{r}',\mathbf{r}'',\omega)}{|\mathbf{r}-\mathbf{r}''|} \\ &\quad \times d^3\mathbf{r}'' + \frac{\partial V_{\text{xc}}(\mathbf{r})}{\partial\rho_{\uparrow}(\vec{r})} \Big|_{\rho_o(\mathbf{r})} \chi_{\uparrow}^{\text{IPA}}(\mathbf{r},\mathbf{r}',\omega), \\ K_{\downarrow\downarrow}(\mathbf{r},\mathbf{r}') &= \int \frac{\chi_{\downarrow}^{\text{IPA}}(\mathbf{r}',\mathbf{r}'',\omega)}{|\mathbf{r}-\mathbf{r}''|} \\ &\quad \times d^3\mathbf{r}'' + \frac{\partial V_{\text{xc}}(\mathbf{r})}{\partial\rho_{\downarrow}(\vec{r})} \Big|_{\rho_o(\mathbf{r})} \chi_{\downarrow}^{\text{IPA}}(\mathbf{r},\mathbf{r}',\omega), \\ K_{\uparrow\downarrow}(\mathbf{r},\mathbf{r}') &= \int \frac{\chi_{\downarrow}^{\text{IPA}}(\mathbf{r}',\mathbf{r}'',\omega)}{|\mathbf{r}-\mathbf{r}''|} d^3\mathbf{r}'', \\ K_{\downarrow\uparrow}(\mathbf{r},\mathbf{r}') &= \int \frac{\chi_{\uparrow}^{\text{IPA}}(\mathbf{r}',\mathbf{r}'',\omega)}{|\mathbf{r}-\mathbf{r}''|} d^3\mathbf{r}''. \end{aligned} \quad (10)$$

The integral equation (9) can now be rewritten as a linear equation, from which  $V_s^{\text{SCF}}(\mathbf{r},\omega)$  can be readily solved by discretization of the  $\mathbf{r}$  space. Substituting the results of

$V_s^{\text{SCF}}(\mathbf{r}, \omega)$  into Eq. (7), we obtain the induced charge density  $\delta\rho(\mathbf{r}, \omega)$ . Finally, the cross section can be obtained by the well-known relationship

$$\sigma(\omega) = \frac{4\pi\omega}{c} \text{Im}[\alpha(\omega)], \quad (11)$$

where  $\alpha(\omega)$  is the dynamical polarizability given by

$$\alpha(\omega) = - \sum_s \int \int V^{\text{ext}}(\mathbf{r}, \omega) \chi_s^{\text{IPA}}(\mathbf{r}, \mathbf{r}', \omega) V_s^{\text{SCF}} \times (\mathbf{r}', \omega) d^3\mathbf{r} d^3\mathbf{r}'. \quad (12)$$

The key issue here is how to calculate the susceptibility based on the IPA potential. Since the susceptibility can be written as a summation over all the orbits, we can calculate the contributions of the susceptibility by the Green's function method as discussed in Ref. [13]. First we rewrite Eq. (6) as

$$\begin{aligned} \chi_s^{\text{IPA}}(\mathbf{r}, \mathbf{r}', \omega) &= \sum_{is, js} n_{is} \frac{\phi_{is}^*(\mathbf{r}) \phi_{js}(\mathbf{r}) \phi_{is}(\mathbf{r}') \phi_{js}^*(\mathbf{r}')}{\omega - (\varepsilon_{js} - \varepsilon_{is}) + i\eta} \\ &\quad - \sum_{is, js} n_{js} \frac{\phi_{is}^*(\mathbf{r}) \phi_{js}(\mathbf{r}) \phi_{is}(\mathbf{r}') \phi_{js}^*(\mathbf{r}')}{\omega - (\varepsilon_{js} - \varepsilon_{is}) + i\eta} \\ &= \sum_{is} n_{is} \phi_{is}^*(\mathbf{r}) \phi_{is}(\mathbf{r}') \sum_{js} \frac{\phi_{js}(\mathbf{r}) \phi_{js}^*(\mathbf{r}')}{\omega - (\varepsilon_{js} - \varepsilon_{is}) + i\eta} \\ &\quad + \sum_{is} n_{is} \phi_{is}(\mathbf{r}) \phi_{is}^*(\mathbf{r}') \sum_{js} \frac{\phi_{js}^*(\mathbf{r}) \phi_{js}(\mathbf{r}')}{\omega - (\varepsilon_{js} - \varepsilon_{is}) - i\eta} \\ &\equiv \sum_{is} n_{is} \phi_{is}^*(\mathbf{r}) \phi_{is}(\mathbf{r}') G(\mathbf{r}, \mathbf{r}'; \omega + \varepsilon_{is} + i\eta) \\ &\quad + \sum_{is} n_{is} \phi_{is}(\mathbf{r}) \phi_{is}^*(\mathbf{r}') G^*(\mathbf{r}, \mathbf{r}'; \varepsilon_{is} - \omega + i\eta) \end{aligned} \quad (13)$$

and then expand the Green's function in terms of spherical harmonics,

$$G(\mathbf{r}, \mathbf{r}'; E) = \sum_L Y_L^*(\hat{\mathbf{r}}) G_L(r, r'; E) Y_L(\hat{\mathbf{r}}'), \quad (14)$$

where  $L$  is a compact notation for the angular momentum quantum numbers  $l, m$ . The radial Greens's function  $G_L(r, r'; E)$  can be determined by

$$G_L(r, r'; E) = \frac{j_l(r_<) h_l(r_>)}{W[j_l, h_l]}, \quad (15)$$

where  $r_<(r_>)$  refers to the smaller (larger) distance of  $r$  and  $r'$ .  $j_l(r)$  is the partial wave solution of Eq. (2) with energy  $E$  and satisfies the proper boundary condition at the origin. Similarly,  $h_l(r)$  is the partial wave solution of Eq. (2) with energy  $E$  and satisfies the outgoing boundary condition as  $r$

$\rightarrow\infty$  for  $E > 0$  or the decaying behavior solution as  $r \rightarrow \infty$  for  $E \leq 0$ .  $W[j_l, h_l]$  is the Wronskian of  $j_l(r)$  and  $h_l(r)$ . With the calculated Green's functions, we can construct the susceptibility from Eq. (13). Once the susceptibility is determined, the self-consistent-field  $V^{\text{SCF}}$  is obtained by the solution of Eq. (9) and the cross section can be calculated by Eqs. (11) and (12). The linear-response method is usually referred to as a *time-dependent* technique. If we use  $V^{\text{EXT}}$  instead of  $V^{\text{SCF}}$  in Eq. (12), we reproduce the cross-section expression for the independent-particle approximation. The independent-particle approximation, Eq. (1), will be referred to as the *time-independent* method since it does not take into account time-dependent field-induced density.

### III. RESULTS AND DISCUSSION

Using the theoretical machinery outlined in the previous section, we calculated the photoabsorption cross section for I,  $\text{I}^+$ ,  $\text{I}^{2+}$ , and  $\text{I}^{3+}$  between 60 and 130 eV. This energy range was used to enable comparison to Amusia *et al.*'s [6] RPAE results and Kjeldsen's [7] experimental results. For all of the species of interest here, this range was sufficient in examining the giant resonance from the  $4d^{10}5d^n$  initial state. Though Kjeldsen *et al.* include data for below 60 eV, this range was not included in the present calculations. This is because the large  $4d \rightarrow 5p$  peak in that region is a transition to an occupied state which is a type of transition not well-suited to treat by the current method. Such transitions are better treated by multiconfiguration Dirac-Fock methods, whereas the strength of the current method rests in its ability to reproduce accurately transitions to the continuum. More importantly, the exclusion of these low excited  $4d^9 5d^{n+1}$  states does not invalidate comparison to experimental results because the experiments are also concerned with single-photon processes. Consequently, two-photon processes such as a  $4d \rightarrow 5p$  transition followed by a transition to the continuum are not considered here. The current calculations do, however, incorporate all single-photon processes from the  $4d$  and  $5p$  channels. In addition, since the current calculations were nonrelativistic, to compare with experimental results, the main peak of the theoretical spectra was matched with the corresponding main peak in the experimental spectra. Also, the spectra for  $\text{I}^+$  and  $\text{I}^{2+}$  were shifted by 1.15 eV and 2.16 eV, respectively. Unless otherwise noted, the theoretical spectra have been convoluted with a 400 meV Lorentzian function.

Figure 1(a) shows the photoabsorption cross section for the  $\text{I}^+$  ion calculated by the LSDA/OEP-SIC method and TDLSDA/OEP-SIC. It should be clear from the plots that the LSDA/OEP-SIC method is not as successful as the TDLSDA method in reproducing the giant resonance. The LSDA/OEP-SIC not only overestimates the size of the resonance but also fails to yield cross-section values that are similar in magnitude to those obtained by the TDLSDA/OEP-SIC method. This finding is consistent with the other studies that have compared the success of LSDA/OEP-SIC against TDLSDA/OEP-SIC [21]. Hence, this result also underscores the point that the giant resonance itself is due to the dynamic electron correlation and its reproduction depends crucially on incor-

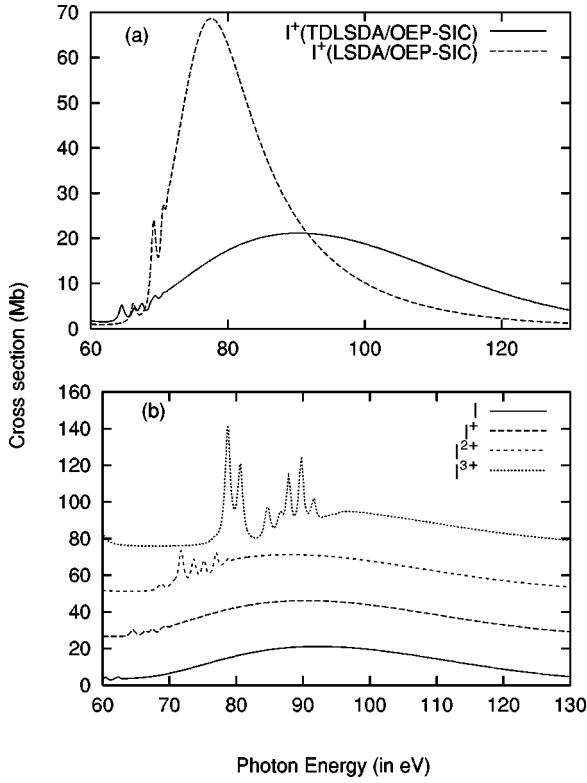


FIG. 1. (a) Photoabsorption cross sections of  $4d$  electrons from  $I^+$  ions using LSDA/OEP-SIC and TDLSDA/OEP-SIC. (b) Calculated photoabsorption cross sections for  $I^-$ ,  $I$ ,  $I^+$ ,  $I^{2+}$ , and  $I^{3+}$ . Each successive spectrum has been shifted upward by 25 Mb.

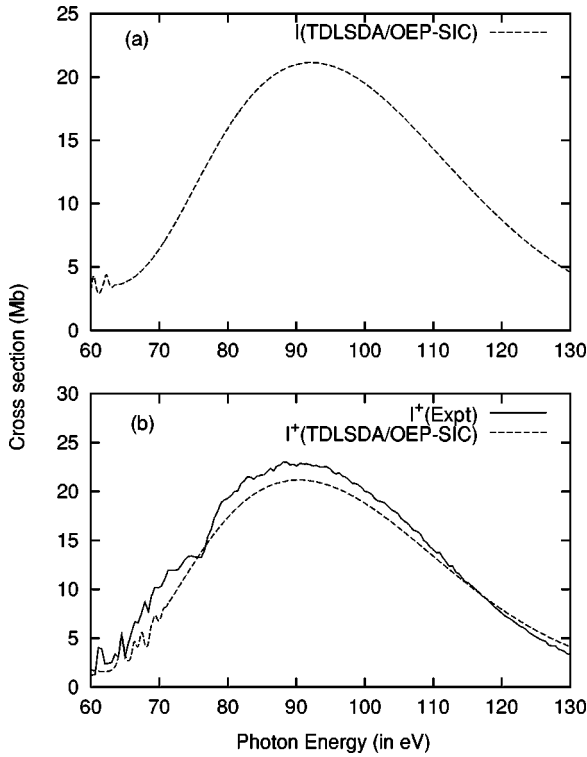


FIG. 2. Photoabsorption spectra for (a)  $I$  atoms and (b)  $I^+$  ions. The experimental spectra are from Kjeldsen *et al.* [7].

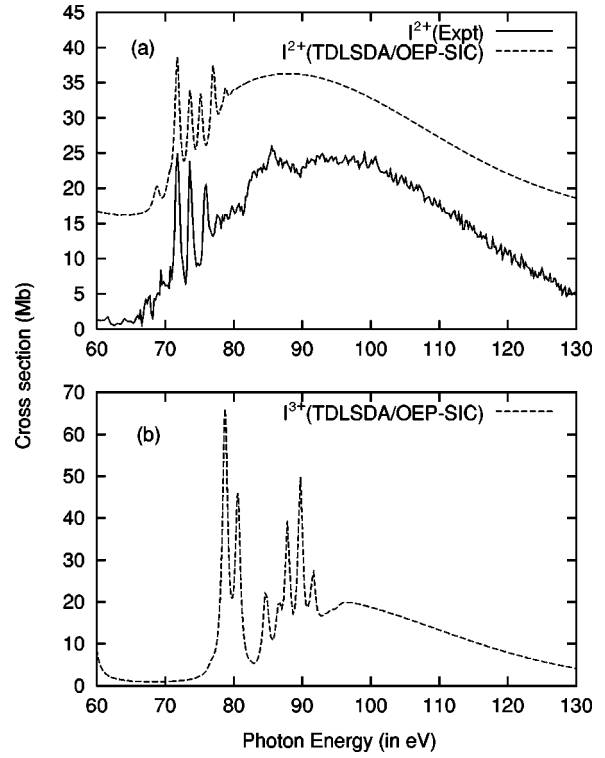


FIG. 3. Photoabsorption spectra for (a)  $I^{2+}$  ions and (b)  $I^{3+}$  ions. Experimental spectra are from Kjeldsen *et al.* [7]. In (a), the theoretical spectra have been shifted upward by 15 Mb.

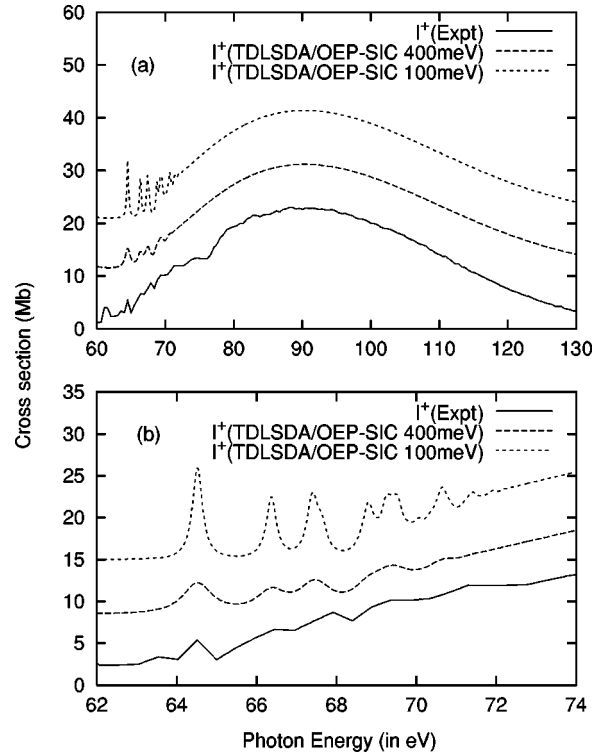


FIG. 4. (a)  $4d$  photoabsorption spectra of  $I^+$  ions convoluted at 100 meV and 400 meV; (b) enlargement of the 62 eV to 74 eV region. Experimental spectra are from Kjeldsen *et al.* [7]. In (a) and (b), each successive theoretical spectrum has been shifted upward by 10 Mb and 7 Mb, respectively.

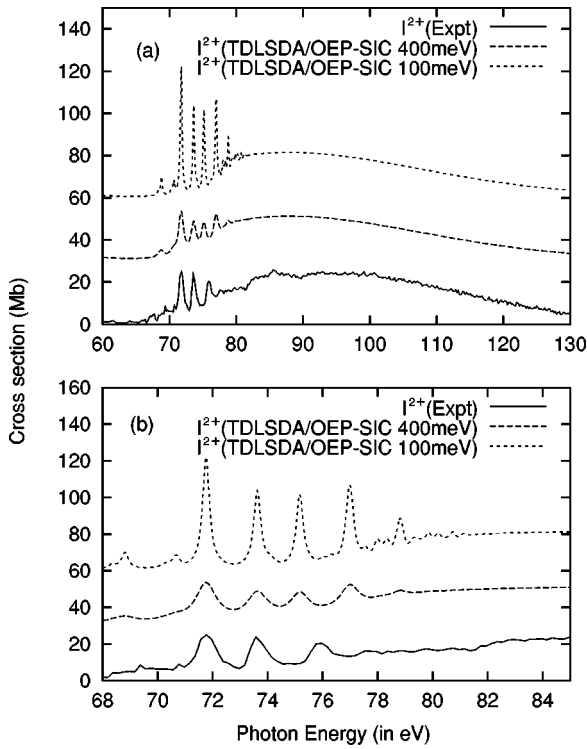


FIG. 5. (a)  $4d$  photoabsorption spectra of  $I^{2+}$  ions convoluted at 100 meV and 400 meV; (b) enlargement of the 68 eV to 85 eV region. Experimental spectra are from Kjeldsen *et al.* [7]. In (a) and (b), each successive theoretical spectrum has been shifted upward by 30 Mb.

porating this effect. Figure 1(b) provides an overview of how the photoabsorption spectrum changes with an increase in the atom's degree of ionization. With higher degrees of ionization, the shape of the atom's photoabsorption spectra alters from one characterized by a giant resonance to one characterized by sharp discrete lines.

Figures 2 and 3 present the spectra for I,  $I^+$ ,  $I^{2+}$ , and  $I^{3+}$ . For species for which experiments have been conducted, our cross-section values agree well with the corresponding experimental data. In particular, Fig. 2(a) indicates the largest photoabsorption cross section for I at about 91 eV. This is in agreement with the relative cross-section values obtained by Nahon [4]. Figure 2(b) shows our cross section values for  $I^+$  together with the absolute experimental values obtained by Kjeldsen *et al.* [7]. Figure 3(a) shows our cross section for  $I^{2+}$  against their values [7]. In both cases, our values fall well within the range of experimental error (10–15%) that Kjeldsen *et al.* give for their experiment [7]. Moreover, our results suggest that the cross-section values obtained by Amusia *et al.* [6] using RPAE overestimates the cross-section values by about 30–40%.

Figure 4 shows the experimental  $I^+$  spectra [7] together with results of convoluting the theoretical spectra with 100 meV and 400 meV Lorentzian functions. Figure 5 shows the same data for the  $I^{2+}$  ion. In addition to the excellent agreement in magnitude and line shape of the theoretical and experimental spectra for both ions, the theoretical spectra suggest that for both ions the experimental resolution may have

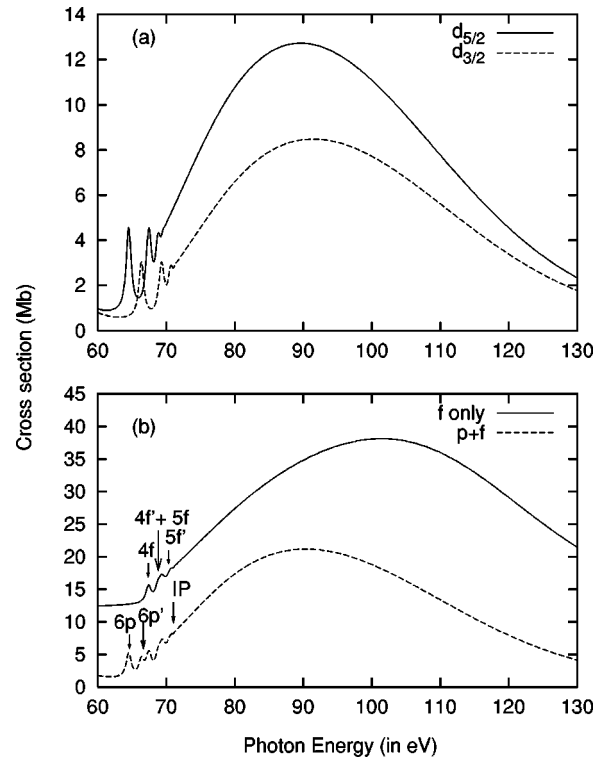


FIG. 6. (a) Decomposition of the photoabsorption spectra of  $I^+$  into its  $4d_{5/2}$  and  $4d_{3/2}$  components. (b) Spectral assignments for the  $I^+$  ion spectra. The  $f$ -only spectrum has been shifted upward by 12 Mb.

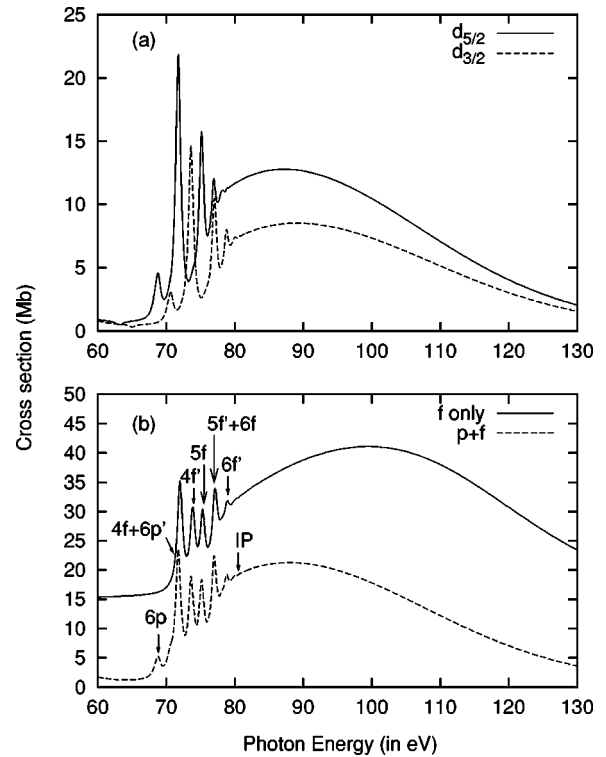


FIG. 7. (a) Decomposition of the photoabsorption spectra of  $I^{2+}$  into its  $4d_{5/2}$  and  $4d_{3/2}$  components. (b) Spectral assignments for the  $I^{2+}$  ion spectra. The  $f$ -only spectrum has been shifted upward by 15 Mb.

been insufficient to resolve some of the discrete lines. This discrepancy is especially clear from Figs. 4(b) and 5(b). In particular, for  $I^+$  the theoretical spectrum employing 100 meV resolution indicates the existence of at least 7 peaks between the 64–72 eV energy range, whereas the experimental spectra resolve clearly only two of these peaks. For  $I^{2+}$ , the theoretical spectrum employing a 100 meV resolution indicates the existence of at least eight peaks between the 70–80 eV range, but the experimental spectra resolve clearly only four of these peaks. Though the experiment employed a photon energy resolution that decreased at a rate of  $E^{5/2}$  starting with 100 meV at 45 eV, these discrepancies suggest the need for an experiment employing a finer resolution. Moreover, it should also be noted that the jaggedness of the broad resonance seen in the experimental spectra is not reproduced in the theoretical spectra. This is because the jaggedness is partly due to multiple small transition probability channels that are not considered in the current calculation.

In addition to comparing the magnitude and shape of the theoretical spectra to the experimental spectra, the spectral peaks were also identified. The assignments were made using a two-step process. First, the fine-structure splitting, which was calculated using relativistic DFT [22], was taken into account by separating the spectra into its  $4d_{5/2}$  and  $4d_{3/2}$  components. For  $I^+$  and  $I^{2+}$  the fine-structure splitting was found to be 1.85 eV and 1.86 eV, respectively. Second, the same spectra were split into transitions to the  $p$  states and transitions to  $f$  states. In practice, contributions to  $f$  states alone were calculated by closing all transition channels to  $p$  states. Transitions to  $p$  states were determined by comparing the full spectra ( $p+f$ ) against the  $f$ -only spectra. Hence, lines present in the former but not in the latter were deduced as transitions to a  $p$  state. In this manner, any sharp peaks appearing before the  $4d$  ionization threshold (denoted by IP

in the figures) were assigned in the systematic manner outlined here. Using the formalism described in the theoretical section, the  $4d$  ionization thresholds for  $I^+$  and  $I^{2+}$  were found to be approximately 71.1 eV and 80.5 eV, respectively.

Figure 6(a) shows the decomposition of the photoabsorption spectra of  $I^+$  into its  $4d_{5/2}$  and  $4d_{3/2}$  components. Figure 6(b) shows the theoretical spectra for  $I^+$  considering the  $f$  and  $p$  partial wave contributions and the spectra due to the  $f$  partial wave alone. Using Figs. 6(a) and 6(b) together enabled determination of all the peaks seen in the theoretical spectra of  $I^+$ . Fig. 7 shows the same information as Fig. 6 but for the  $I^{2+}$  ion. As seen in Fig. 7(a), decomposing the photoabsorption spectra of  $I^{2+}$  into its  $4d_{5/2}$  and  $4d_{3/2}$  components yielded the expected monotonic decrease in peak intensity in moving from the  $4f$  to  $6f$  peaks. Figures 7(a) and 7(b) together also bring attention to the fact that the  $4d_{3/2} \rightarrow 5f$  peak and the  $4d_{5/2} \rightarrow 6f$  peak are in the same position. This accounts for the five rather than the expected six peaks  $f$  peaks that one might expect due to the splitting of the  $4f$ ,  $5f$ , and  $6f$  peaks. A similar situation is seen with regard to the  $4d_{3/2} \rightarrow 6p$  peak because the  $4d_{3/2} \rightarrow 6p$  peak is in the same position as the much larger  $4d_{5/2} \rightarrow 4f$  peak. Hence, this accounts for why only the  $4d_{5/2} \rightarrow 6p$  peak is immediately identifiable from the splitting of the  $4d \rightarrow 6p$  peak.

In summary, we have calculated the photoionization cross-section  $4d$  electrons for  $I$ ,  $I^+$ ,  $I^{2+}$ , and  $I^{3+}$  between 60 and 130 eV using linear density-response theory and density-functional theory with an optimized effective potential and self-interaction correction. Our results are in good agreement with experiment and thereby suggest that the RPAE results overestimate the cross sections by 30–40%. In addition, the peaks in the theoretical spectra of  $I^+$  and  $I^{2+}$  were identified. Finally, the presence of some peaks in the theoretical spectra that were absent in the corresponding experimental spectra suggests the need for a higher-resolution experiment [23].

- 
- [1] T. Hayaishi *et al.*, J. Phys. B **17**, 3511 (1984).  
 [2] F. Combet-Franoux, in *Giant Resonance in Atoms, Molecules and Solids*, edited by J. P. Connerade, J. E. Esteve, and R. C. Karnatak (Plenum, New York, 1986).  
 [3] J. P. Connerade, J. E. Esteve, and R. C. Karnatak, *Giant Resonance in Atoms, Molecules and Solids* (Plenum, New York, 1986).  
 [4] L. Nahon, A. Svensson, and Paul Morin, Phys. Rev. A **43**, 2328 (1991).  
 [5] G. O'Sullivan, C. McGuinness, J.T. Costello, E.T. Kennedy, and B. Weinmann, Phys. Rev. A **53**, 3211 (1996).  
 [6] M.Y. Amusia *et al.*, Phys. Rev. A **61**, 020701(R) (2000).  
 [7] H. Kjeldsen *et al.*, Phys. Rev. A **62**, 020702 (2000).  
 [8] K.T. Cheng and W.R. Johnson, Phys. Rev. A **28**, 2820 (1983).  
 [9] M.Y. Amusya, K.V. Ivanov, and V.A. Kupchenko, Z. Phys. D: At., Mol. Clusters **14**, 219 (1989).  
 [10] X.M. Tong, J.M. Li, and R.H. Pratt, Phys. Rev. A **42**, 5348 (1990).  
 [11] X.M. Tong, Acta Phys. Sin. **40**, 693 (1991).  
 [12] X.M. Tong, D. Kato, T. Watanabe, and S. Ohtani, J. Phys. B **33**, 717 (2000).  
 [13] A. Zangwill and P. Soven, Phys. Rev. A **21**, 1561 (1980).  
 [14] E. Runge and E.K.U. Gross, Phys. Rev. Lett. **52**, 997 (1984).  
 [15] E.K.U. Gross and W. Kohn, Phys. Rev. Lett. **55**, 2850 (1985).  
 [16] G. D. Mahan and K. R. Subbaswamy, *Local Density Theory of Polarizability* (Plenum Press, New York, 1990).  
 [17] M. Stener, P. Decleva, and A. Lisini, J. Phys. B **28**, 4973 (1995).  
 [18] A. Fetter and J. Walecka, *Quantum Theory of Many-Body Systems* (McGraw-Hill, New York, 1971).  
 [19] X.M. Tong and S.I. Chu, Phys. Rev. A **55**, 3406 (1997).  
 [20] J. Chen, J. Krieger, Y. Li, and G. Iafrate, Phys. Rev. A **54**, 3939 (1996).  
 [21] X. M. Tong, M. Sato, T. Watanabe, and S. Ohtani (unpublished).  
 [22] X.M. Tong and S.I. Chu, Phys. Rev. A **57**, 855 (1998).  
 [23] T. Andersen (private communication).